Ballistic electron transmission in out-of-plane crossed wire junctions



1994 J. Phys.: Condens. Matter 6 1731

(http://iopscience.iop.org/0953-8984/6/9/014)

J. Phys.: Condens. Matter 6 (1994) 1731–1738. Printed in the UK

# Ballistic electron transmission in out-of-plane crossed wire junctions

Y Takagaki and K Ploog
Paul-Drude-Institut für Festkörperelektronik, Hausvogteiplatz 5-7, 10117 Berlin, Germany

Received 20 October 1993

**Abstract.** We have performed quantum-mechanical and classical simulations of ballistic electron transport in three-dimensional waveguide structures. The considered geometries are cross junctions of two out-of-plane waveguides, in which the coupling between the waveguides takes place in the third direction, perpendicular to the orthogonal waveguide axes. We find that the transmission coefficients in the single-mode regime are strongly affected by quantum-mechanical interferences of scattering due to directional conversions during the transmission. A large modulation of straight-through transmission is achieved by varying the aspect ratio of the cross section of the waveguides. The transmission into the side leads is found to disappear over a wide range of sample parameters. The magnetic-field dependence of the transport is also examined within the classical limit.

## 1. Introduction

A considerable number of experimental and theoretical studies has been made on ballistic electron transport in quantum-wire structures in recent years [1]. In the arguments presented so far, electrons are assumed to be restricted to a two-dimensional (2D) plane of infinitesimal thickness. The 2D plane is then patterned to simulate the wire structures. The assumption of true two-dimensionality was reasonable since the width of the wires fabricated by the microfabrication technologies was considerably larger than the thickness of the two-dimensional electron gas (2DEG) confined at the interface of GaAs–AlGaAs heterojunctions. Consequently, only the lowest mode is occupied below the Fermi energy for the confinement perpendicular to the heterointerface, whereas several modes are typically occupied when the lateral confinement is concerned. Because of the recent advances of microfabrication technologies, the wire width can now be reduced to be comparable with the thickness of 2DEGs. Using advanced crystal-growth methods, it has been demonstrated that the wire width can be controlled on the order of atomic layer precision [2]. In samples of these dimensions, the thickness of the channels need to be treated on an equal footing with the width. Furthermore, using further advanced technologies, such as combined focused ion-beam implantation and regrowth technique [3], it will become feasible to construct three-dimensional (3D) quantum-wire structures, in which a rich variety of quantum-mechanical effects can be expected to take place.

Recently, the quantum-mechanical electron transmission in a 3D out-of-plane cross junction has been investigated [4]. Two waveguides extending in two orthogonal directions are placed on top of each other as illustrated in figure 1 so that the coupling between them takes place in the direction perpendicular to the terminal waveguides. It was found that resonant structures are superimposed on the transmission in contrast to the conventional 2D junction [4], in which no transmission resonances appear if the junction consists of

0953-8984/94/091731+08$19.50  

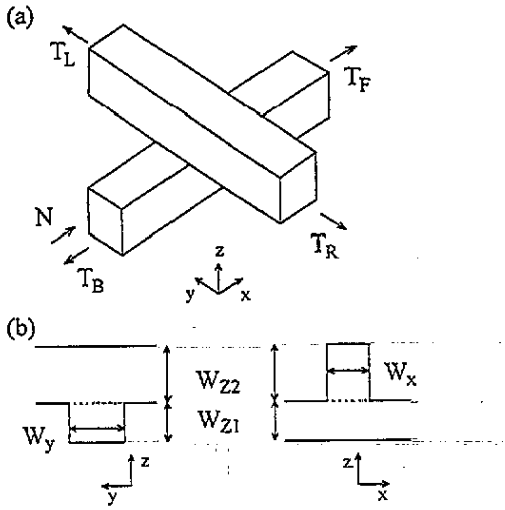


**Figure 1.** (*a*) Schematic view of the out-of-plane crossed-wire junction. Because of the symmetry of the structure, transmission probabilities into each end of the upper waveguide are identical in the absence of magnetic field. (*b*) Cross-sectional views of the two waveguides. The bottom of the upper waveguide is attached to the top of the lower waveguide.

straight waveguides [5]. Surprisingly, the transmission into the side leads was found to be absent over a wide range of energy in the single-mode regime [4]. The two waveguides are effectively decoupled and thus the 3D cross junction behaves, in a sense, as if it were an insulator when the bend resistance [6] is measured. In the simulation of [4] the widths of the waveguides were assumed to be identical.

It is the purpose of this paper to describe the transmission properties when inequivalent channel widths are assumed. We show that the transmission through the incident waveguide is modified between fairly good transparency and significant opaqueness in the single-mode regime as the ratio of the channel widths is varied. The variation is much larger than the classical prediction and manifests a remarkable quantum-mechanical influence due to the attachment of the second waveguide. We also examine the magnetotransport properties within the classical limit. We find that the four-terminal resistances in the structure exhibit a very weak magnetic-field dependence due to rebound and guiding effects.

## 2. Numerical model

We take the electrostatic potential to be zero within the channel and infinite outside. The window between the two waveguides is assumed to be completely transparent. Let us first consider the case in the absence of a magnetic field, for simplicity. Suppose that an electron with energy $E_F = \hbar^2 k_F^2/2m$ is incident through the lower waveguide. The electron is either transmitted in the forward direction with probability $T_F$ or into each end of the side leads with probability $T_S (= T_L = T_R)$ or reflected with probability $T_B$. We define the transmission coefficients such that probability conservation reads

$$T_F + T_L + T_R + T_B = N \tag{1}$$

where $N$ is the number of propagating modes in the incident waveguide. In a waveguide of widths $W_y$ and $W_{z1}$, $N$ is roughly given by $\pi E_F/4E_{unit}$ with $E_{unit} = \pi^2\hbar^2/2mW_yW_{z1}$. The transmission coefficients are determined by employing a waveguide-matching technique [7]. For comparison, we also calculate the classical transmission coefficients by a billiard model [8]. Electrons are injected into the sample with velocity $v_F = (2mE_F)^{1/2}$. A uniform distribution over the channel width and a cos $\theta$ dependence of the angular distribution

on the incident angle $\theta$ in $x$–$y$ and $x$–$z$ planes are used to estimate the transmission coefficients, which are then determined by counting the number of classical trajectories leaving the sample through each terminal lead [9]. The clearest quantum-mechanical effects are expected in the single-mode regime so that we restrict our discussion to the single-mode regime. The average quantum transmission approaches the classical limit as the number of occupied modes is increased [4]. Details of the scattering properties essentially depend on particular choices of the channel widths, and the transmission drastically changes as higher-lying modes are occupied below $E_F$ in any of the terminal leads. Therefore, although the purpose of this paper is to examine cases of inequivalent channel widths, we assume for simplicity that the two waveguides have a geometrically identical cross section. This also ensures simultaneous population of the modes in both waveguides.

## 3. Quantum transmission in the single-mode regime

The transmission coefficients for the identical-channel-width case, $W_x = W_y = W_{z1} = W_{z2} \equiv W$, are shown in figure 2 as a function of the Fermi energy. The energy is normalized to the threshold energies for the lowest and the second modes as $\epsilon = (E_F - E_1)/(E_2 - E_1)$, where $E_1 = \pi^2\hbar^2/2mW^2$ and $E_2 = 4E_1$. One finds three transmission resonances in the single-mode regime at $\epsilon = 0.6, 0.93$, and $0.997$ (labelled A, B, and C, respectively). At the resonances A and C, all the transmission coefficients become roughly identical; $T_F \sim T_S \sim T_B \sim \frac{1}{4}$. On the other hand, the electron is nearly completely reflected at the resonance B, resembling the transmission resonances in two-terminal narrow–wide–narrow (NWN) geometries [10]. This behaviour can be explained in terms of parity of the quasi-bound states relevant to the resonances [5]. In the limit of weak coupling between the terminal leads and the intersection region, the quasi-bound state energies are given by

$$E_{n,m,l} = (n\pi/W_x^{\text{eff}})^2 + (m\pi/W_y^{\text{eff}})^2 + (l\pi/[W_{z1} + W_{z2}])^2 \qquad (2)$$

where $W_x^{\text{eff}} \geqslant W_x$ and $W_y^{\text{eff}} \geqslant w_y$ are the effective widths of the intersection region in the $x$- and $y$-directions, respectively. Evaluating the probability distribution at the resonances, we find that the resonances A and B are respectively associated with the quasi-bound states $(n, m, l) = (1, 1, 3)$ and $(2, 1, 2)$ with $W_x^{\text{eff}} \sim W_y^{\text{eff}} \sim 1.15W$. For the quasi-bound state corresponding to the resonance C, the free boundary is found to be playing a crucial role, and thus the resonance C cannot be characterized by equation (2). The propagating mode in the side leads can couple to the even-parity (in the $x$-direction) quasi-bound state A, whereas it does not couple to the odd-parity state B if the symmetry of the structure is exact. Hence, the incident electron exits through all the out-going states with equal probabilities for the resonance A. On the other hand, the resonance B does not disturb $T_S$ and, as a consequence, the sample can be regarded as the two-terminal NWN junction when odd-parity resonances, such as the resonance B, are concerned. Notice that a transmission resonance corresponding to $(2, 1, 1)$, which is naively expected to have a lower resonance energy than $(2, 1, 2)$, does not show up in figure 2. We ascribe this to the fact that $W_x^{\text{eff}}$ and $W_y^{\text{eff}}$ are restricted to $W$ in the window region, where the probability distribution takes the maximum in the $z$-direction. The resonance energy is, hence, pushed away above the threshold of the second mode.

The transmission coefficients are plotted in figures 3 and 4 for various aspect ratios $\alpha \equiv W_{z1}/W_y$ of the cross section of the waveguides. We assume $W_x = W_y$ and $W_{z2} = W_{z1}$ for figure 3, and so the two waveguides have exactly the same cross section. One finds that $T_F$ is, in general, suppressed while $T_B$ is enhanced as the waveguide becomes horizontally wide. The classical values for the transmission coefficients, which are indicated by the

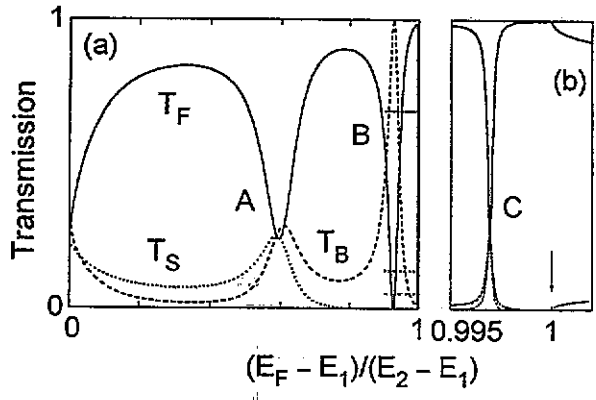


**Figure 2.** (*a*) Transmission coefficients when equivalent waveguide widths are assumed are plotted as a function of normalized energy in the single-mode regime. Three transmission resonances are labelled A, B, and C, respectively. The horizontal lines indicate the values for the classical transmission. Transmission coefficients into the four leads become nearly identical at the resonances A and C, while almost complete backscattering takes place at the resonance B. (*b*) The resonance C is shown with expanded energy scale. The arrow indicates the threshold of the second mode ($\epsilon = 1$). The electron is incident only through the lowest mode, and so the total transmission probability for $\epsilon > 1$ is unity.

horizontal lines, also show this behaviour. However, the enhancement of the backscattering is more pronounced in the quantum-mechanical case. In the classical case, $T_F(T_B)$ varies from 0.54 (0.09) to 0.81 (0.02) as $\alpha$ is increased from 0.5 to 2, whereas the straight-through transmission in the quantum-mechanical case exhibits more than 80% modulation over a wide range of energy in the single-mode regime. We note that $T_S$ and $T_B$ have an interesting relation in the quantum-mechanical case when $\alpha$ is increased. They become almost identical over the entire energy range in the single-mode regime.

The cross section of the upper waveguide is rotated at right angles for figure 4, i.e. $W_x = W_{z1}$ and $W_{z2} = W_y$. Note that the symmetry of the transmission requires the $T_S$ for $\alpha = \alpha_0$ in figure 4(*a*) to be identical with the $T_S$ for $\alpha = 1/\alpha_0$ in figure 4(*b*). The classical calculation indicates that the transmission in this case is almost independent of $\alpha$. However, the quantum-mechanical results again show the enhancement of $T_B$ and suppression of $T_F$ when $\alpha$ is decreased, though the trend is less clear compared to the previous case. We thus conclude that the enhanced backscattering depends largely on the aspect ratio of the incident waveguide. The ratio of the area of the window region to that of the waveguide cross section is $1/\alpha$ in the case shown in figure 3, whereas it is unity in the case shown in figure 4. The number of electrons entering the upper waveguide and eventually being scattered increases with decreasing $\alpha$ in the former case, whereas it is held constant in the latter case. This explains the behaviour of the classical transmission. In the quantum-mechanical situation, the transverse momentum component of the electrons is increased in the vertical direction when the waveguide is vertically narrowed, provided that the number of occupied modes is unchanged. The electrons will suffer strong scattering from the upper waveguide in this case, leading to the quantum-mechanical enhancement of the backscattering.

The transmission resonances are shifted in energy as the cross section of the waveguides is modified. In general, the resonance energies should be increased in the normalized scale as the aspect ratio deviates from unity since the increase of the confinement energy in the narrower direction is dominant rather than the decrease in the other direction. The decrease of the normalized resonance energies for the $W_x > W_{z2}$ cases is thus somehow

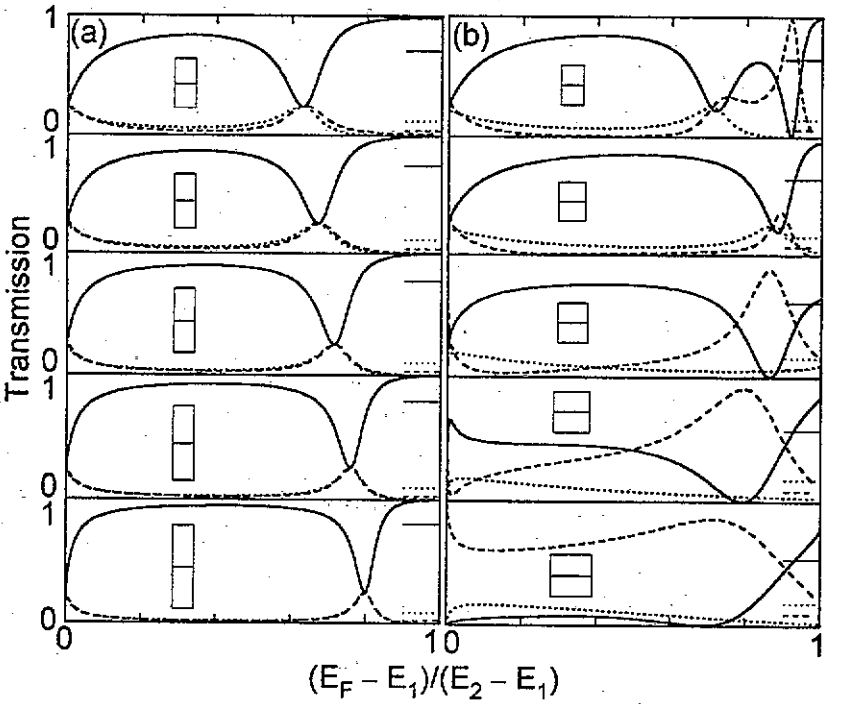


**Figure 3.** Transmission coefficients, $T_F$ (solid line), $T_S$ (dotted line), and $T_B$ (dashed line), are plotted as a function of normalized energy for various aspect ratios $\alpha = W_{z1}/W_y$ when $W_x = W_y$ and $W_{z2} = W_{z1}$. The values of $\alpha$ from the top panel to the bottom one are (*a*) 1.2, 1.4, 1.6, 1.8, and 2.0 and (*b*) 0.9, 0.8, 0.7, 0.6, and 0.5. The horizontal lines indicate the values for the classical transmission. The insets illustrate cross sections of the waveguides.

unexpected. As a consequence, the resonances A and B cross each other. This is ascribed to the open boundary of the intersection region. Notice that the transmission coefficients at the resonance A are not identical in figure 4 since the four terminal leads are no longer symmetric. Interestingly, the shape of the resonance A changes to become similar to that of the even-parity resonance and $T_S$ becomes independent of the resonance as $\alpha$ is increased in figure 4(*b*), though we find that the resonance is still associated with the (1, 1, 3) quasi-bound state. This is because the quasi-bound state with $l = 3$ effectively possesses even parity in the $z$-direction within the cross section of the upper waveguide when $W_{z1}/W_{z2} = 0.5$. The coupling of the incident mode with the resonance state A is weakened for the same reason in figure 4(*a*) when $W_{z1}/W_{z2}$ approaches two. We assume that additional resonances originating from the quasi-bound states that do not couple with the propagating modes due to parity in the symmetric structure will emerge in the transmission in the presence of disorder.

Below the threshold for propagation of the excited mode, $T_S$ exhibits a nearly complete absence over a wide energy range [4]. This results in a divergence of the bend resistance $R_B$, in which two adjacent leads are used as current source and sink, i.e., a current flows from one waveguide to the other, and the voltage difference is measured between the other two leads [6], since $R_B$ is related to the transmission coefficients as [11]

$$R_B = (h/2e^2)(T_F - T_S)/4T_S(T_S + T_F). \tag{3}$$

Our results indicate that the quenching of $T_S$ appears over a wide range of the sample

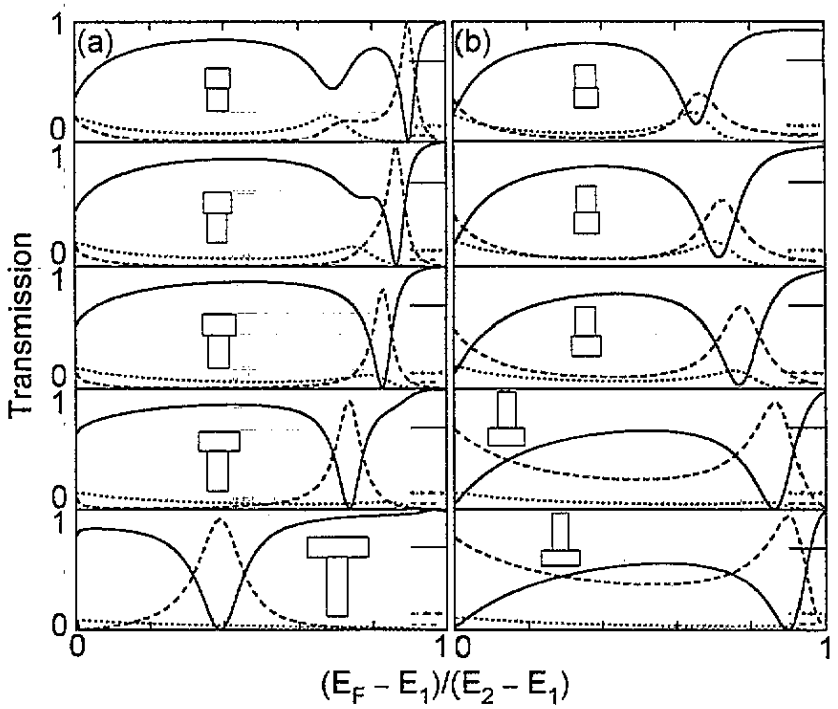


**Figure 4.** Solid, dotted, and dashed lines indicate respectively transmission coefficients $T_F$, $T_S$, and $T_B$ for various ratios of the widths of the waveguides when $W_x = W_{z1}$ and $W_{z2} = W_y$. The cross sections of the waveguides are rotated at right angles to each other as illustrated by the insets. The values of $\alpha$ from the top panel to the bottom one are ($a$)1.2, 1.4, 1.6, 2.0, and 3.0 and ($b$) 0.9, 0.8, 0.7, 0.5, and 0.4. The horizontal lines indicate the values for the classical transmission.

parameters and is a generic property of the 3D cross junction. The single-mode transport is crucial for the quenching phenomenon and $T_S$ is not quenched in the multi-mode regime even if the electron is incident *only* through the lowest mode as shown in figure 2($b$). Generally, the quenching appears in the energy range above the resonance A. Therefore, the energy range of the quenching takes the maximum in the normalized scale as the aspect ratio is unity.

## 4. Classical magnetotransmission

We now consider the effects of a magnetic field $B$ applied parallel to the $z$-axis on the transmission properties. The direction of the magnetic field is chosen such that the Lorentz force deflects electrons to increase $T_L$ at the expense of $T_F$ as well as $T_R$. To evaluate the transmission probabilities in the semi-classical limit, we extended the method of Beenakker and van Houten [8] to the 3D geometry. The electrons are injected from a lead, in which $B$ is assumed to be zero, attached to the intersection region so as to allow us to use the same injection distribution as employed for the $B = 0$ case. Note that, in any realistic simulation, it is required that rounded corners are taken into account, which will lead to a variety of anomalous behaviours in the weak-field Hall resistance [8,9]. However, we neglect the smooth corners to concentrate on the effects of the 3D nature of the geometry on the magnetotransport properties.

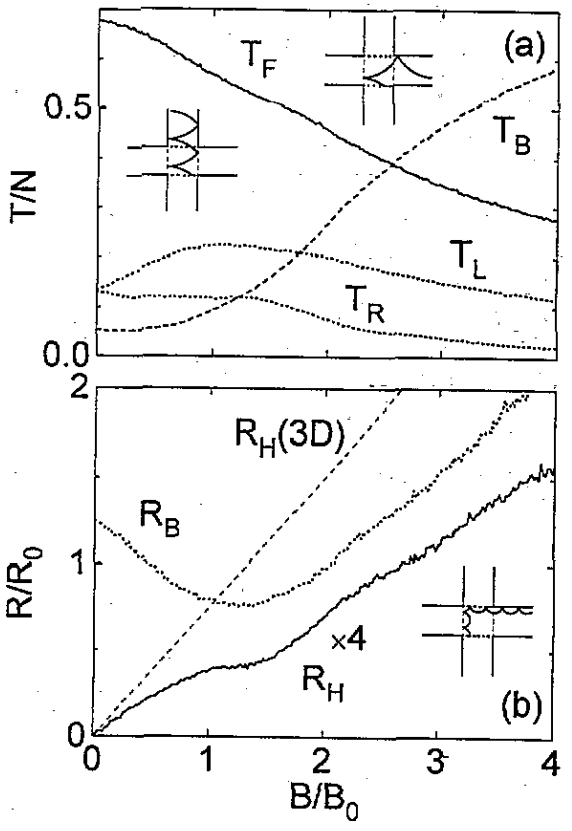


**Figure 5.** (*a*) Transmission coefficients are plotted as a function of magnetic field for the identical-channel-width case. The insets illustrate guiding and rebound trajectories. (*b*) Hall resistance and bend resistance calculated from the transmission coefficients in (*a*). The conventional Hall resistance $R_H/R_0 = \frac{3}{4}B/B_0$ in a 3D in-plane cross junction is indicated by the dashed line. The inset illustrates a trajectory that leads electrons to the right side probe in high magnetic fields.

In figure 5(*a*), we show the transmission coefficients normalized by the total flux $N = (\pi/4)(k_F W/\pi)^2$ as a function of magnetic field. (The widths of the channels are assumed to be identical.) The normalization factor for the magnetic field is $B_0 \equiv \hbar k_F/eW$. The Hall resistance $R_H$ and the bend resistance $R_B$ calculated from the transmission coefficients as [11]

$$R_H = (h/2e^2)(T_L - T_R)/[(T_F + T_L)^2 + (T_F + T_R)^2] \tag{4}$$

$$R_B = (h/2e^2)(T_F^2 - T_L T_R)/(T_L + T_R)[(T_F + T_L)^2 + (T_F + T_R)^2] \tag{5}$$

are plotted in figure 5(*b*). Here, the resistances are normalized by $R_0 \equiv h/2Ne^2$. At low magnetic fields, $T_L$ increases and $T_R$ decreases monotonically as $B$ is increased, resulting in the nearly linear dependence of $R_H$ around zero field. The value of $R_H$ is, however, significantly smaller than that in a 3D in-plane cross junction (dashed line). This can be explained in terms of guiding and rebound trajectories in the out-of-plane cross junction. Because of the configuration of the waveguides, many electrons are guided into the forward lead along the side walls of the incident waveguide (left inset in figure 5(*a*)) or reflected from the side wall into the wrong Hall probe (top inset in figure 5(*a*)) [12]. These trajectories are responsible for the suppression of $T_L$ and the enhancement of $T_R$. When the diameter of the cyclotron orbit $2\hbar k_\perp/eB$, where $k_\perp$ is the magnitude of the wave vector transverse to the magnetic field, becomes less than $W$, the rebound trajectories cease to exist. The transmission $T_R$ into the right side lead is suppressed for $B > 2B_0$ compared to the low-field regime since no orbits intersect both opposite side walls. We note, however, that some electrons are still led into the right side probe in high magnetic fields due to the

trajectories illustrated in the inset of figure 5(*b*). The transmission coefficients are averaged over the cyclotron diameter because of continuous $z$-component of electron momentum in the classical limit. Therefore, the magnetoresistance reveals less clear features around the critical magnetic field $B_c = 2B_0$ in the 3D case compared to the 2D case.

Let us discuss $R_B$, in which the guiding effect is particularly highlighted. Because of preferential forward transmission in the ballistic regime, $R_B$ takes a finite value at $B = 0$ [6]. As shown in figure 5(*b*), $R_B$ is suppressed in weak magnetic fields as the straight-through trajectories are destroyed. The $R_B$ in the out-of-plane cross junction obviously takes non-zero values over an extremely wide range of $B$ due to the guiding. Furthermore, $R_B$ is, in contrast to the 2D case, enhanced for $B > B_c$, where the cyclotron orbits cannot reach the forward and the right side leads in the in-plane junction (and hence $R_B = 0$). The ratios of $T_F$, $T_L$, and $T_R$ are found to be roughly independent of $B$ for $B > B_c$. The electron motion in the $z$-direction is not influenced by the perpendicular magnetic field, and so the main effect of $B$ in this strong-field regime is to increase a fraction $T_B$ (i.e., to decrease the effective total flux $N - T_B$ that contributes to the transmission process), resulting in the enhancement of $R_B$ (since the resistance is inversely proportional to the amount of flux).

## 5. Conclusions

We have presented classical and quantum-mechanical transmission properties in out-of-plane cross junctions in the single-mode regime. The quantum transmission is drastically modified as the aspect ratio of the cross section is varied, indicating the importance of the quantum-mechanical nature of geometrical scattering. The transmission coefficients exhibit a very weak magnetic-field dependence within the classical limit due to rebound and guiding trajectories in the out-of-plane geometry. The bend resistance is found to be enhanced in strong magnetic fields.

## Acknowledgment

The authors wish to thank M Wassermeier for a critical reading of the manuscript.

## References

[1] For a review see Beenakker C W J and van Houten H 1991 *Solid State Physics* vol 44, ed H Ehrenreich and D Turnbull (New York: Academic) p 1
[2] Gaines M, Petroff P M, Kroemer H, Geels R S and English J H 1988 *J. Vac. Sci. Technol.* B **6** 1378
Pfeiffer L N, West K W, Stormer H L, Eisenstein J P, Baldwin K W, Gershoni D and Spector J 1990 *Appl. Phys. Lett.* **56** 1697
Däweritz L, Hagenstein K and Schützendübe P 1993 *J. Vac. Sci. Technol.* A **11** 1802
[3] Hashimoto H 1990 *Semiconductors and Semimetals* vol 29, ed T Ikoma (San Diego: Academic) p 63
[4] Takagaki Y and Ploog K 1993 *Phys. Rev.* B **11** 508
[5] Schult R L, Ravenhall D G and Wyld H W 1989 *Phys. Rev.* B **39** 5476
[6] Takagaki Y, Gamo K, Namba S, Takaoka S, Murase K, Ishibashi K and Aoyagi Y 1988 *Solid State Commun.* **68** 1051
[7] Takagaki Y and Ferry D K 1992 *Phys. Rev.* B **45** 12 152
[8] Beenakker C W J and van Houten H 1989 *Phys. Rev. Lett.* **63** 1857
[9] Baranger H U, DiVincenzo D P, Jalabert R A and Stone A D 1991 *Phys. Rev.* B **44** 10 637
[10] Sols F, Macucci M, Ravaioli U and Hess K 1989 *J. Appl. Phys.* **66** 3892
[11] Büttiker M 1986 *Phys. Rev. Lett.* **57** 1761
[12] Ford C J B, Washburn S, Büttiker M, Knoedler C M and Hong J M 1989 *Phys. Rev. Lett.* **62** 2724